

# Convergence and Stability of Biochemical Reaction Systems of Rank One

Mihaela Sbarciog\*

Mia Loccufier\*

Erik Noldus\*

\* Department of Electrical Energy, Systems and Automation, Ghent University, Technologiepark 913, B-9052 Ghent, Belgium  
 Phone: 32-(0)9-264 5584, Fax: 32-(0)9-264 5839, E-mail: mihaela@autoctrl.UGent.be

**Abstract**—The dynamics of biochemical reaction systems of rank one are studied. The global convergence of the set of equilibrium points is investigated and the local stability properties of the equilibria are analysed. The problem of stability boundary estimation is addressed and an algorithm for the visualization of the boundaries is proposed. The theoretical results and the effectiveness of the proposed algorithms are verified by two examples.

## I. INTRODUCTION

A biochemical reaction system is a process defined by a set of  $m$  biochemical reactions involving  $n$  components, with  $n > m$ . The process takes place in a reactor vessel which we assume to operate in a continuous mode: Substrates are fed to the system continuously while an effluent stream is continuously withdrawn from it, such that the culture volume remains constant. The system dynamics can be encoded into a reaction network, described by a characteristic matrix of constant yield coefficients [1], [2]. The rank of this matrix is often called the rank of the reaction network [3].

Although most of the techniques developed below can, to some extent, be generalized to a reactor in which several biochemical reactions take place, we shall in this paper concentrate on basic concepts, using process models involving a single biochemical reaction. In this case, the characteristic matrix consists of a single vector  $c \in R^n$  of rank one and the reactor dynamics can generally be cast in the form:

$$\dot{\xi} = cr(\xi) - D\xi + F - Q \quad (1)$$

In (1),  $\xi$ , of dimension  $n$ , is the composition vector of the reactor. It is the vector of concentrations of the various components participating to the process, such as populations of microorganisms, enzymes, external substrates fed to the reactor, components produced by the reaction, all expressed in units of mass per unit of reactor volume.  $\xi$  constitutes the state vector of the system.

$F = col(F_i; i = 1 \dots n)$  and  $Q = col(Q_i; i = 1 \dots n)$  represent the vectors of supply rates, respectively rates of removal in gaseous form of the components per unit of volume. They satisfy:

$$F_i \geq 0; \quad Q_i \geq 0; \quad i = 1 \dots n \quad (2)$$

$D$  is a positive scalar. It is called the specific volumetric outflow rate or dilution rate. In uncontrolled reactors  $F$  and  $D$  are constant.

We assume that

$$F_i - Q_i \geq 0 \quad \text{if } \xi_i = 0; \quad i = 1 \dots n \quad (3)$$

$r(\xi)$  is the reaction rate function, in units of mass per unit of time  $\times$  unit of volume. Let  $r(\xi) \in C^1$  (continuous with continuous partial derivatives w.r.t. the components of  $\xi$ ). This condition ensures the existence and the uniqueness of the solutions of (1) for given initial conditions. We assume that for all values of the composition vector  $\xi$ ,

$$r(\xi) \geq 0 \quad (4)$$

Furthermore we assume that  $r(\xi)$  can be written as

$$r(\xi) = \mu(\xi) \prod_i^l \xi_i \quad (5)$$

such that  $r(\xi) = 0$  if  $\xi_i = 0$ .  $l$  is the number of reactants which are consumed in the reaction.

$c = col(c_i; i = 1 \dots n)$  is the vector of yield coefficients (dimensionless and constant). The  $i^{th}$  entry of  $c$  satisfies:  $c_i > 0$  if the  $i^{th}$  component is produced in the reaction and  $c_i < 0$  if it is consumed.  $r(\xi)$  can be normalized in such a way that at least one coefficient  $c_i$  either equals 1 or -1.

It is easy to show [2] that under fairly weak and physically plausible conditions the state variables of the system (1) cannot become negative and remain upper bounded for increasing time [4]. Along the system's solutions we have:

$$\xi_i(0) \geq 0 \implies 0 \leq \xi_i(t) \leq \xi_{imax} < +\infty; \quad \forall t \geq 0, \quad i = 1 \dots n \quad (6)$$

Relationship (6) expresses that the model (1) is a positive system. We define  $R^{+n} \triangleq \{\xi \in R^n; \xi_i \geq 0; i = 1 \dots n\}$  as its state space.

## II. CONVERGENCE

As the reaction rate function displays various types of process inhibition effects, the system (1) usually possesses at least two stable equilibrium points, one of which corresponds to the normal operating point of the process and the other one to a wash out state, where all or almost all biological activity in the vessel has disappeared. In addition, there may exist one or more unstable equilibria.

In this section we determine the global convergence of the set of the equilibrium points. A system which has this property may be called a nonoscillatory system. Nonoscillatory systems cannot exhibit complicated motions such as periodic motions, other types of sustained oscillations or chaotic behaviour. As time increases every solution settles down in one of the system's equilibrium states.

Since  $\text{rank } c = 1$  we can assume, without loss of generality, that  $c_1 \neq 0$ . Then an equivalent canonical state representation [1] of system (1) can be obtained by letting

$$x_1 \stackrel{\Delta}{=} \xi_1 \quad (7)$$

$$x_i \stackrel{\Delta}{=} \xi_i - \frac{c_i}{c_1} \xi_1 ; \quad i = 2 \dots n \quad (8)$$

With these notations, system (1) becomes:

$$\dot{x}_1 = D(w_1 - x_1) + c_1 \rho(x) \quad (9)$$

$$\dot{x}_i = D(w_i - x_i) ; \quad i = 2 \dots n \quad (10)$$

where

$$\rho(x) = r(\xi)|_{\xi_1=x_1; \xi_i=x_i+\frac{c_i}{c_1}x_1; i=2\dots n} \quad (11)$$

$$w_1 = \frac{1}{D}(F_1 - Q_1) \quad (12)$$

$$w_i = \frac{1}{D} \left[ (F_i - Q_i) - \frac{c_i}{c_1} (F_1 - Q_1) \right]; i = 2 \dots n \quad (13)$$

The analysis of system (9), (10) dynamics, using basic Lyapunov theory, leads to the following result:

**Theorem 1 :** As  $t \rightarrow +\infty$  every solution of the system (9), (10) converges to an equilibrium point.

This result has been proven in [4], where

$$V(x) \stackrel{\Delta}{=} \frac{1}{2} a \sum_{i=2}^n (w_i - x_i)^2 + \int_0^{x_1} \varphi(\theta) d\theta ; \quad a > 0 \quad (14)$$

has been considered as a candidate Lyapunov function, with

$$-\varphi(x_1) \stackrel{\Delta}{=} D(w_1 - x_1) + c_1 \rho_0(x_1) \quad (15)$$

$$\rho_0(x_1) \stackrel{\Delta}{=} \rho(x)|_{x_i=w_i; i=2\dots n} \quad (16)$$

### III. STABILITY

In this section we investigate the local stability properties of equilibrium points and we discuss the geometric structure of the stability boundaries of locally asymptotically stable equilibria.

The equilibrium points of the system (9), (10) are

$$x = \hat{x}_i = [\hat{x}_{i1} \quad w_2 \quad \dots \quad w_n]' ; \quad i = 1 \dots p \quad (17)$$

where  $\hat{x}_{i1}$  is a solution of  $\varphi(x_1) = 0$ . The equilibria have the following properties:

- Since by Theorem 1, every solution converges to an equilibrium point, the system has at least one equilibrium state. If there is an unique equilibrium state  $\hat{x}_1$ , then it is globally convergent.
- The system's Jacobian at  $\hat{x}_i$  is:

$$J(\hat{x}_i) = \begin{bmatrix} -D + c_1 \frac{\partial \rho}{\partial x_1} & c_1 \frac{\partial \rho}{\partial x_2} & \dots & c_1 \frac{\partial \rho}{\partial x_n} \\ & -D & & \\ & & \ddots & \\ & & & -D \end{bmatrix} \quad (18)$$

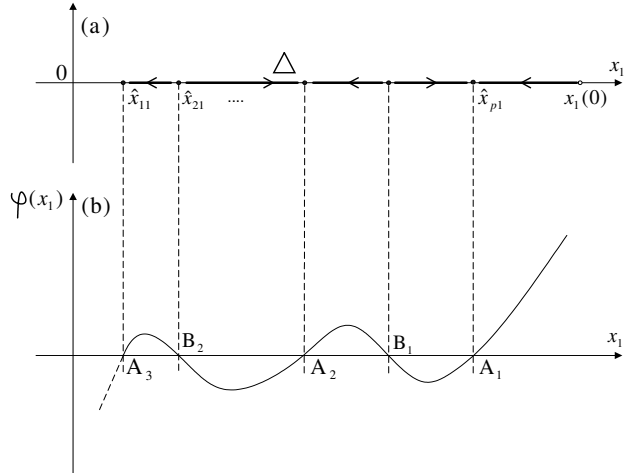


Fig. 1. Systems dynamics on the straight half line  $\Delta$

with eigenvalues:

$$\lambda_{i1} = \left[ -D + c_1 \frac{\partial \rho(\hat{x}_i)}{\partial x_1} \right] = \left[ -D + c_1 \frac{d\rho_0}{dx_1} \right]_{x_1=\hat{x}_{i1}} \quad \lambda_{i2} = -D < 0.$$

We shall assume that all equilibrium points are hyperbolic, i.e.  $J(\hat{x}_i)$  has no eigenvalues on the imaginary axis. Then  $\lambda_{i1} \neq 0$ ;  $i = 1 \dots p$ .

- Consider the solutions on the straight half line  $\Delta \stackrel{\Delta}{=} \{x; x_1 \geq 0, x_i = w_i, i = 2 \dots n\}$ :

$$x(t) = [x_1(t) \quad w_2 \quad \dots \quad w_n]'$$

where according to (9), (15):

$$\dot{x}_1 = -\varphi(x_1) \quad (19)$$

Fig. 1a displays an example of a phase portrait of system (19). In the situation depicted in Fig. 1b the slope of  $\varphi(x_1) \in C^1$  is positive in  $A_1$  and nonzero in  $A_2, A_3, \dots, B_1, B_2, \dots$ . It follows that for the system (9), (10) the equilibrium points are either locally asymptotically stable (l.a.s.), with index 0, or unstable, with index 1. Moreover, the system's solutions remain bounded for increasing time, therefore the equilibrium point with the largest  $x_1$ -value is l.a.s. The l.a.s. equilibrium points alternate with the unstable equilibrium points on the  $\Delta$ -axis.

- If on  $\Delta$  there is no equilibrium point at  $x_1 = 0$ , then  $\dot{x}_1 \neq 0$  at  $x = [0 \quad w_2 \quad \dots \quad w_n]'$ . However  $\dot{x}_1 = \dot{\xi}_1 \geq 0$  for  $x_1 = \xi_1 = 0$ , thus

$$\dot{x}_1 > 0 \quad \text{for } x_1 = 0 \quad (20)$$

From (20) we conclude that the equilibrium point  $\hat{x}_1$  with the smallest  $x_1$ -value is l.a.s.

If on  $\Delta$  there is an equilibrium point at  $x_1 = 0$ , then it can be either l.a.s. or unstable.

If an equilibrium point  $\hat{x}_i$  is l.a.s. it possesses a region of attraction  $\Omega(\hat{x}_i)$  and a stability boundary  $\partial\Omega(\hat{x}_i)$  which are proper subsets of the state space. The stability boundary

is invariant. Crucial in its geometric characterization is the concept of transversality. Let  $\hat{x}_j$  and  $\hat{x}_k$  be two equilibrium states. Let  $x(t, x_0)$  be the solution with initial state  $x_0$  at  $t = 0$ . The unstable manifold

$$W^u(\hat{x}_j) \triangleq \{x_0; \quad x(t, x_0) \rightarrow \hat{x}_j \text{ as } t \rightarrow -\infty\}$$

and the stable manifold

$$W^s(\hat{x}_k) \triangleq \{x_0; \quad x(t, x_0) \rightarrow \hat{x}_k \text{ as } t \rightarrow +\infty\}$$

satisfy the transversality condition [6] if either

$$W^u(\hat{x}_j) \cap W^s(\hat{x}_k) = \emptyset, \quad \text{or}$$

$$T_x[W^u(\hat{x}_j)] + T_x[W^s(\hat{x}_k)] = R^n; \quad (21)$$

$$\forall x \in W^u(\hat{x}_j) \cap W^s(\hat{x}_k)$$

Relationship (21) means that the tangent spaces of  $W^u(\hat{x}_j)$  and  $W^s(\hat{x}_k)$  at the intersection point  $x$  span the entire  $R^n$ -space.

It is easy to see that the transversality condition holds for the stable and unstable manifolds of two equilibria of the system (9), (10). In fact if  $\hat{x}_j$  and  $\hat{x}_k$  are unstable equilibria on  $\partial\Omega(\hat{x}_i)$  then  $W^u(\hat{x}_j)$  and  $W^s(\hat{x}_k)$  do not intersect. In view of the above, the system (9), (10) has the following properties:

- All equilibrium points are hyperbolic.
- Every trajectory on  $\partial\Omega(\hat{x}_i)$  approaches an equilibrium point as  $t \rightarrow +\infty$ .
- The stable and unstable manifolds of the equilibrium points on  $\partial\Omega(\hat{x}_i)$  satisfy the transversality condition.

As a result of these three properties, we have:

**Theorem 2** (Theorem 3.7 in [6]):

$$\hat{x}_j \in \partial\Omega(\hat{x}_i) \text{ if and only if } W^u(\hat{x}_j) \cap \Omega(\hat{x}_i) \neq \emptyset \quad (22)$$

**Theorem 3** (Theorem 4.1 in [6]):

$$\partial\Omega(\hat{x}_i) = \bigcup_{\hat{x}_j \in \partial\Omega(\hat{x}_i)} W^s(\hat{x}_j) \quad (23)$$

In biochemical reactor dynamics, modelling the reaction rate functions  $r(\xi)$  and identifying the system parameters is often a difficult and hazardous task. Therefore it is worth noting that the structural properties discussed above remain valid irrespective the mathematical expressions of the reaction kinetics and the numerical values of the model parameters. These properties are inherent to the basic structure of the canonical representation (9), (10).

#### IV. ESTIMATION AND VISUALIZATION OF STABILITY BOUNDARIES

The estimation of a stability boundary  $\partial\Omega(\hat{x}_i)$  involves two steps. First the index 1 equilibria lying on  $\partial\Omega(\hat{x}_i)$  must be determined. For this purpose we can use Theorem 2. Subsequently for each one of these equilibria, say  $\hat{x}_k \in \partial\Omega(\hat{x}_i)$ , an estimate  $W^s(\hat{x}_k)_{est}$  of  $W^s(\hat{x}_k)$  must be computed, such that  $W^s(\hat{x}_k)_{est} \subset \Omega(\hat{x}_i)$  and  $W^s(\hat{x}_k)_{est} \rightarrow W^s(\hat{x}_k)$  for some algorithmic parameter  $\varepsilon \rightarrow 0$ .

$W^s(\hat{x}_k)_{est}$  can be used in (23) to construct an estimated stability boundary, in principle of any desired accuracy, lying inside  $\Omega(\hat{x}_i)$ . This estimate  $\partial\Omega(\hat{x}_i)_{est}$  surrounds a stability region  $\Omega(\hat{x}_i)_{est} \subset \Omega(\hat{x}_i)$ . Numerical algorithms for these problems, in particular trajectory reversing techniques, have been extensively described in literature [7].

Furthermore the problem arises of visualizing the stability boundaries in the case of models of order higher than three. A possible visualization technique consists of computing intersections of  $\partial\Omega(\hat{x}_i)_{est}$  with well selected hyperplanes in the state space. The effectiveness of the numerical procedures may be substantially improved by exploiting the special structure of the bioreactor model (9), (10) which contains a linear time invariant subsystem of order  $(n-1)$ .

##### A. Estimation of the stability boundary

For simplicity, we translate  $\hat{x}_k$  to the origin of the state space:

$$x = \hat{x}_k + z \quad (24)$$

Since  $\hat{x}_k$  is an equilibrium point, the system (9), (10) becomes:

$$\dot{z}_1 = -Dz_1 + c_1 [\rho(\hat{x}_k + z) - \rho(\hat{x}_k)] \triangleq -\psi(z) \quad (25)$$

$$\dot{z}_i = -Dz_i; \quad i = 2 \dots n \quad (26)$$

The equilibrium points of (25), (26) are:

$$\begin{aligned} \hat{z}_k &= 0 \\ \hat{z}_i &= \hat{x}_i - \hat{x}_k; \quad i = 1 \dots p; \quad i \neq k \end{aligned}$$

To determine  $W^s(\hat{x}_k)_{est}$  by trajectory reversing a suitable anchor set  $\gamma$  of initial states  $z_0$  is needed for integrating the system (25), (26) in reverse time. Let

$$\gamma \triangleq \{z_0; \quad z_{01} = \varepsilon \operatorname{sgn}(\hat{z}_{i_1}); \quad a_0^2(z_{02}^2 + \dots + z_{0n}^2) = \varepsilon^2\} \quad (27)$$

where  $\varepsilon > 0$  and  $a_0 > 0$ . If  $\varepsilon$  is sufficiently small and  $a_0$  sufficiently large, then  $\gamma \subset \Omega(\hat{z}_i)$ , since  $\Omega(\hat{z}_i)$  is an open set. Next, letting  $\tau \triangleq -t$ , (26) yields:

$$z_i(\tau) = e^{D\tau} z_{0i}; \quad i = 2 \dots n \quad (28)$$

while from (25) we obtain

$$\frac{dz_1}{d\tau} = \psi_0(z_1, z_{02}, \dots, z_{0n}, \tau); \quad z_1(0) = z_{01} \quad (29)$$

where

$$\psi_0(z_1, z_{02}, \dots, z_{0n}, \tau) \triangleq \psi(z)|_{z_1(\tau)=e^{D\tau} z_{01}}; \quad i=2\dots n$$

Expression (28) and the solution of the first order differential equation (29), where  $0 \leq \tau < \infty$  and where the initial conditions  $z(0) = z_0 \in \gamma$ , together with the cone segment connecting  $\gamma$  with  $\hat{z}_k = 0$ , define the manifold  $W^s(\hat{z}_k)_{est}$ . We have

$$W^s(\hat{z}_k)_{est} \rightarrow W^s(\hat{z}_k) \text{ as } \varepsilon \xrightarrow{\rightarrow} 0$$

### B. Visualization of the stability boundary

For  $n \geq 3$  we can visualize the estimated stability boundary by computing intersections of  $W^s(\hat{z}_k)_{est}$  with one or more hyperplanes  $\alpha$ :

$$\alpha \triangleq \{z ; z_i = \eta_i ; i = 3 \dots n\} \quad (30)$$

Suppose a trajectory in  $W^s(\hat{z}_k)_{est}$ , computed in reverse time, intersects  $\alpha$  at  $\tau = \tau_f$ . Let  $z(\tau_f) = z_f = \text{col}(z_{f_i}; i = 1 \dots n)$ . Then from (28) we have

$$z_{0_i} = e^{-D\tau_f} \eta_i ; i = 3 \dots n$$

Hence, as  $z_0 \in \gamma$ :

$$a_0^2(z_{f_2}^2 + \eta_3^2 + \dots + \eta_n^2) = (\varepsilon e^{D\tau_f})^2$$

or

$$z_{f_2}^2 = \left[ \frac{\varepsilon}{a_0} e^{D\tau_f} \right]^2 - (\eta_3^2 + \dots + \eta_n^2) \quad (31)$$

For given  $\varepsilon > 0$ ,  $a_0 > 0$ ,  $\eta_3, \dots, \eta_n$  compute  $\tau_{f_{min}}$  such that

$$\frac{\varepsilon}{a_0} e^{D\tau_{f_{min}}} = (\eta_3^2 + \dots + \eta_n^2)^{\frac{1}{2}} \quad (32)$$

Then for any  $\tau_f \geq \tau_{f_{min}}$  we have

$$z_{0_2} = \pm \sqrt{\left( \frac{\varepsilon}{a_0} \right)^2 - (\eta_3^2 + \dots + \eta_n^2)} e^{-2D\tau_f} \triangleq \begin{cases} z_{0_{2,1}} \\ z_{0_{2,2}} \end{cases} \quad (33)$$

Next, solving (29) for  $0 \leq \tau \leq \tau_f$ , using the obtained expressions for  $z_{0_2} \dots z_{0_n}$  allows us to find  $z_{f_1} = z_1(\tau_f)$ . The points  $z_{f_1}$  and

$$z_{f_2} = \pm \left\{ \left[ \frac{\varepsilon}{a_0} e^{D\tau_f} \right]^2 - (\eta_3^2 + \dots + \eta_n^2) \right\}^{\frac{1}{2}}$$

for  $\tau_{f_{min}} \leq \tau_f < \infty$  determine the desired intersection line.

Note that for  $\tau_f = \tau_{f_{min}}$ ,  $z_{f_2} = 0$  and  $z_2(\tau) \equiv 0$ . For each  $\tau_f > \tau_{f_{min}}$  two points  $(z_{f_1}, z_{f_2})$  are obtained. Hence the intersection line  $W^s(\hat{z}_k)_{est} \cap \alpha$  in the  $z_1 - z_2$ -plane consists of two segments joined together at  $z_2 = 0$ .

The visualization procedure described above has the disadvantage that the state variables  $z_i$  do not have a simple physical meaning. However, visualizations represented in  $z$ -space can be numerically transformed to visualizations in  $\xi$ -space using straightforward transformation techniques.

### C. Further analysis of the anchor set

The condition  $\gamma \subset \Omega(\hat{z}_i)$  requires that  $\varepsilon$  is chosen sufficiently small and  $a_0$  sufficiently large. In the following we determine a lower bound for the parameter  $a_0$  by making use of the system's Lyapunov function.

Using (24) and (14) the quadratic approximation of  $V(x) - V(\hat{x}_k)$  in the neighbourhood of the equilibrium point  $x = \hat{x}_k$  is readily obtained as:

$$V(x) - V(\hat{x}_k) = \frac{1}{2} a \sum_{i=2}^n z_i^2 - \frac{1}{2} \left[ c_1 \frac{d\rho_0(\hat{x}_{k_1})}{dx_1} - D \right] z_1^2 \quad (34)$$

where

$$\left[ c_1 \frac{d\rho_0(x_1)}{dx_1} - D \right]_{x_1=\hat{x}_{k_1}} = - \frac{d\varphi(x_1)}{dx_1} \Big|_{x_1=\hat{x}_{k_1}} > 0 \quad (35)$$

since  $\hat{x}_k$  is unstable. Next, we write  $\dot{V}(x)$  in the neighbourhood of  $x = \hat{x}_k$  as:

$$\begin{aligned} \dot{V}(x) = & - \sum_{i=2}^n \left[ \frac{a}{D} \dot{z}_i^2 + \frac{c_1}{D} \frac{\partial \rho(x)}{\partial x_i} \Big|_{x=\hat{x}_k} \dot{z}_i \dot{z}_1 + \eta_i^2 \dot{z}_1^2 \right] \\ & - \left[ 1 - \sum_{i=2}^n \eta_i^2 \right] \dot{z}_1^2 \end{aligned} \quad (36)$$

$\dot{V}(x)$  is negative definite in the neighbourhood of  $z = 0$  if

$$\sum_{i=2}^n \eta_i^2 < 1 \text{ and } \left[ \frac{c_1}{D} \frac{\partial \rho(x)}{\partial x_i} \Big|_{x=\hat{x}_k} \right]^2 < \frac{4a}{D} \eta_i^2 \quad (37)$$

This can be satisfied if

$$a > \frac{c_1^2}{4D} \sum_{i=2}^n \left[ \frac{\partial \rho(x)}{\partial x_i} \Big|_{x=\hat{x}_k} \right]^2 \quad (38)$$

Choose  $\gamma$  as the intersection of the surface  $\{x ; V(x) - V(\hat{x}_k) = 0\}$  with the plane:

$$z_1 = \varepsilon \text{sgn}(\hat{z}_{i_1}) \quad (39)$$

Then  $\gamma$  assumes the form (27), where in order to satisfy (38) we must take

$$a_0 > \frac{\frac{c_1^2}{4D} \sum_{i=2}^n \left[ \frac{\partial \rho(x)}{\partial x_i} \Big|_{x=\hat{x}_k} \right]^2}{\left[ c_1 \frac{d\rho_0(x_1)}{dx_1} - D \right]_{x_1=\hat{x}_{k_1}}}. \quad (40)$$

Define

$$G \triangleq \left\{ z ; \text{sgn}(z_1) = \text{sgn}(\hat{z}_{i_1}); V(x) - V(\hat{x}_k) \leq 0; z_2^2 + \dots + z_n^2 \leq \frac{\varepsilon^2}{a_0^2} \right\}$$

Then  $\gamma \subset G$ . Choose  $\varepsilon > 0$  and sufficiently small, such that the disk  $\{z ; z_1 = \hat{z}_{i_1}, z_2^2 + \dots + z_n^2 \leq \frac{\varepsilon^2}{a_0^2}\}$  lies in the region of attraction of the l.a.s. equilibrium point  $\hat{z}_i$ . Now it is a simple geometrical exercise to show that a solution starting on  $\gamma$  cannot leave the set  $G$  and for  $t \rightarrow +\infty$  must converge to  $\hat{z}_i$ . So  $\gamma \subset \Omega(\hat{z}_i)$ . Equation (40) yields the lower bound for  $a_0$ .

## V. EXAMPLE

Consider a simple model of a fermentation process of the form (1), with  $n = 3$  and  $m = 1$ , where  $\xi_1$ ,  $\xi_2$  and  $\xi_3$  respectively represent biomass, substrate and product concentrations. Let  $c = [c_1 \ c_2 \ c_3]'$ ,  $c_1 > 0$ ,  $c_2 < 0$ ,  $c_3 > 0$ ,  $F = [0 \ F_2 \ 0]'$ ,  $F_2 > 0$ ,  $Q = 0$  and  $r(\xi)$  a Haldane type reaction rate function of the form:

$$r(\xi) = \mu_m \frac{\xi_2}{K_p + \xi_2 + \frac{\xi_2^2}{K_i}} \xi_1; \quad \mu_m, K_p, K_i > 0. \quad (41)$$

The corresponding system representation (9), (10) has an equilibrium point  $\hat{x}_1 = [0 \ w_2 \ 0]'$ ,  $w_2 = F_2/D$ , which represents a situation of complete wash-out. It is easy to show that for dilution rates in the interval  $D_{min} < D < D_{max}$ , with

$$\begin{aligned} D_{min} &= c_1 \mu_m \frac{w_2}{K_p + w_2 + \frac{w_2^2}{K_i}} \\ D_{max} &= \frac{c_1 \mu_m}{1 + 2\sqrt{\frac{K_p}{K_i}}} \end{aligned}$$

there are two additional equilibria: an unstable index 1 equilibrium point  $\hat{x}_2$  and a l.a.s. equilibrium point  $\hat{x}_3$  corresponding to the reactor's normal operating state. The numerical values of the model parameters are:  $c = [1 \ -1.2 \ 0.5]'$ ,  $\mu_m = 4.1 h^{-1}$ ,  $K_p = 2000 g/l$ ,  $K_i = 5 g/l$ ,  $D = 0.05 h^{-1}$ ,  $F_2 = 25 g/hl$ . The equilibrium points are:

$$\hat{\xi}_1 = \begin{bmatrix} 0 \\ 500 \\ 0 \end{bmatrix} \quad \hat{\xi}_2 = \begin{bmatrix} 101.18 \\ 378.59 \\ 50.59 \end{bmatrix} \quad \hat{\xi}_3 = \begin{bmatrix} 394.65 \\ 26.41 \\ 197.33 \end{bmatrix} \quad (42)$$

In  $z$ -space they are given by:

$$\hat{z}_1 = \begin{bmatrix} -101.18 \\ 0 \\ 0 \end{bmatrix} \quad \hat{z}_2 = \begin{bmatrix} 0 \\ 0 \\ 0 \end{bmatrix} \quad \hat{z}_3 = \begin{bmatrix} 293.48 \\ 0 \\ 0 \end{bmatrix} \quad (43)$$

Since (1) is a positive system, several physical boundary conditions in  $z$ -space must be fulfilled:

$$\begin{cases} z_1 + 101.18 \geq 0 \\ z_2 - 1.2z_1 + 378.59 \geq 0 \\ z_3 + 0.5z_1 + 50.59 \geq 0 \end{cases} \quad (44)$$

The stability boundary separating the regions of attraction of  $\hat{z}_1$  and  $\hat{z}_3$  is  $W^s(\hat{z}_2)$ . An estimate of the stability boundary  $W^s(\hat{z}_2)_{est} \subset \Omega(\hat{z}_3)$  is obtained by applying the trajectory reversing technique described in Section IV.

Fig. 2 illustrates the phase portrait of the system in the  $z_1 - z_2$ -plane ( $z_3 \equiv 0$ ). The simulation results are in accordance with Theorem 1: Every trajectory converges to an equilibrium point. All trajectories starting on the physical boundary line  $z_1 + 101.18 = 0$  converge to the wash-out equilibrium point  $\hat{z}_1$ . Trajectories starting on the physical boundary line  $z_2 - 1.2z_1 + 378.59 = 0$ , for some initial conditions, will converge to the wash-out state. For other initial conditions they will converge to the operating point  $\hat{z}_3$ .

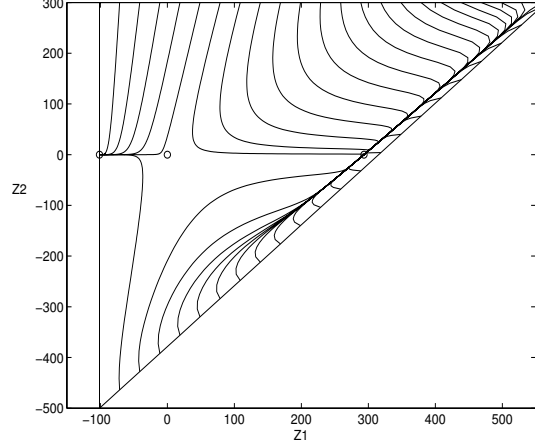


Fig. 2. The phase portrait of the system in the  $z_1 - z_2$ -plane

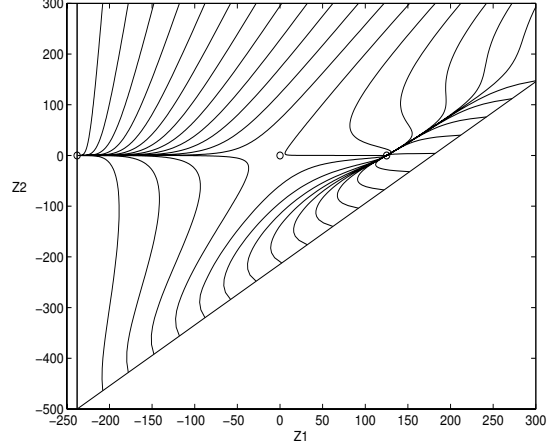


Fig. 3. The phase portrait in the  $z_1 - z_2$ -plane of the system with product inhibition

For this example, the intersections of  $\partial\Omega(\hat{z}_3)$  with any plane  $\{z_3 = \eta_3\}$  are identical to the curve  $W^s(\hat{z}_2)$  in the  $z_1 - z_2$ -plane. This is due to the fact that  $z_3$  does not influence the dynamics of  $z_1$  and  $z_2$ .

The example can be extended to the case where product inhibition occurs. Then, the reaction rate function changes to:

$$r(\xi) = \mu_m \frac{\xi_2}{K_p + \xi_2 + \frac{\xi_2^2}{K_i}} \frac{P}{P + \xi_3} \xi_1 \quad (45)$$

Let  $P = 220 g/l$ .

Product inhibition modifies the position of the equilibrium points. For the selected value of  $P$ , the phase portrait of the system in the  $z_1 - z_2$ -plane ( $z_3 \equiv 0$ ) and the new equilibrium points are illustrated in Fig. 3.

Product inhibition also has an impact on the shape of the stability boundary. Intersections with planes  $\{z_3 = \eta_3\}$  now provide different curves in the  $z_1 - z_2$ -plane as shown in Fig. 4. The representation in the  $\xi_1 - \xi_2$ -plane is depicted in Fig. 5, where the dashed line corresponds to the example without product inhibition.

The influence of the kinetic coefficient  $P$  on the shape of

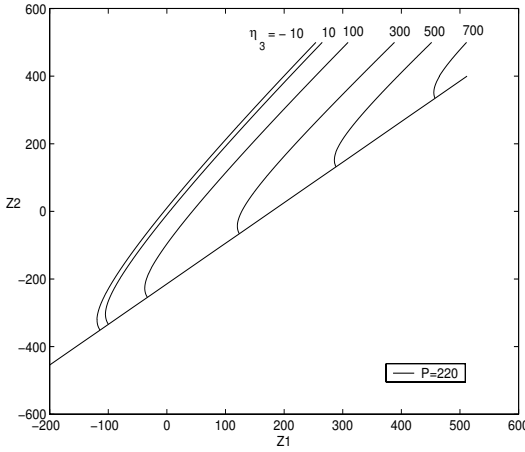


Fig. 4. Intersections of the stability boundary with different planes  $z_3 = \eta_3$  for the case with product inhibition

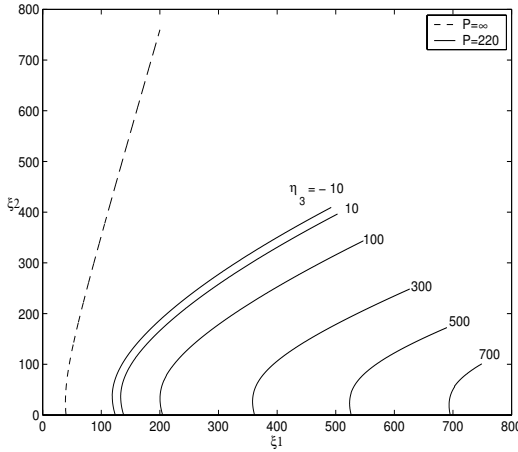


Fig. 5. Intersections of the stability boundary represented in the  $\xi_1 - \xi_2$  plane

the stability boundary is shown in Fig. 6, where intersections of the stability boundaries corresponding to various values of  $P$  with the same plane  $z_3 = \eta_3 = 100$  are represented in the  $\xi_1 - \xi_2$ -plane. For increasing  $P$ , the stability boundary straightens out and approaches the stability boundary of the system without product inhibition ( $P = \infty$ ). This is in accordance with the observation that for high values of  $P$ , the reaction rate function (45) becomes (41) and the inhibitory effect of the product disappears.

## VI. CONCLUSIONS

In this work fundamental properties regarding the convergence and stability of biochemical reaction systems of rank one have been established. These properties hold generally, independent of the structure of the kinetics.

The special form of the canonical model has been exploited to fully characterize the geometric structure of the operating point's stability boundary in state space. Numerically accurate and robust algorithms to evaluate this boundary have been presented.

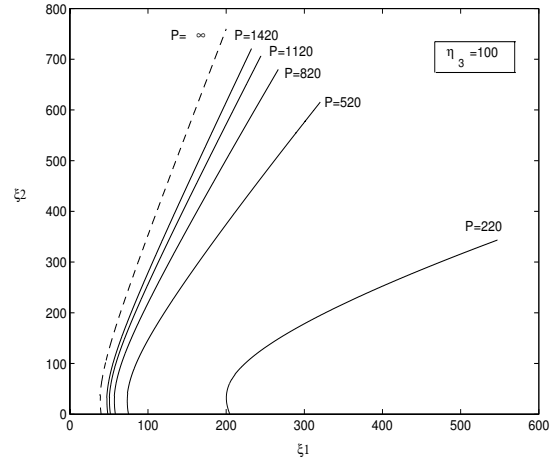


Fig. 6. Influence of the product inhibition kinetic coefficient on the stability boundary

Furthermore, an algorithm that allows to visualize the extent of the stability regions in a high dimensional state space has been developed. This algorithm consists of computing intersections of the stability boundary with well-selected hyperplanes in state space.

The advantage of these algorithms lies in the fact that they do not require any iterative procedures. They yield stability boundary estimates, which can approach the true stability boundary with arbitrary accuracy. Even for large values of the dynamical order  $n$ , they involve a limited numerical effort.

The proposed tools for analysis and estimation of the stability boundary can also be applied to biochemical reaction systems of higher rank. However in such cases additional complications will occur [8].

Future developments may involve the application of the aforementioned analysis and stability boundary estimation techniques to specific industrial systems. The effect of feedback on stability will also be investigated.

## REFERENCES

- [1] G. Bastin and J. F. Van Impe, "Nonlinear and adaptive control in biotechnology: a tutorial", *European Journal of Control*, vol. 1, pp. 37-53, 1995.
- [2] G. Bastin and D. Dochain, *On-line Estimation and Adaptive Control of Bioreactors*, Amsterdam: Elsevier, 1990.
- [3] M. Feinberg, "Chemical reaction network structure and the stability of complex isothermal reactors", Rev. Art. 25 *Chemical Engineering Science*, vol. 42, pp. 2229-2268, 1987.
- [4] M. Sbarciog, M. Loccuifur, E. Noldus, "Global convergence and stability properties of a class of biochemical reactor systems", In: *Proceedings of VIII triennial Int. SAUM Conf. on Systems, Automatic Control and Measurements*, Belgrade, pp. 34-41, 2004.
- [5] H. K. Khalil, *Nonlinear Systems*, 2nd ed., New Jersey: Prentice-Hall, 1996.
- [6] H. D. Chiang, M. W. Hirsch and F. F. Wu, "Stability regions of nonlinear autonomous dynamical systems", *IEEE Trans. on Auto. Control*, vol. 33, pp. 16-27, 1988.
- [7] M. Loccuifur and E. Noldus, "A new trajectory reversing method for estimating stability regions of autonomous nonlinear systems", *Nonlinear Dynamics*, vol. 21, pp. 265-288, 2000.
- [8] M. Sbarciog, M. Loccuifur, E. Noldus, "The computation of stability boundaries in state space for a class of biochemical engineering systems", In: *Proceedings of Third Int. Conf. on Advanced Computational Methods in Engineering*, Ghent, 12p., 2005.